ACS Catalysis

pubs.acs.org/acscatalysis
Research Article

Reversed TiO_x Layer-Induced Strong Metal–Support Interactions on Ni/Ti–SiO_2 Catalysts for Propene Epoxidation with H_2 and O_2

Defu Yin, Dong Lin,* Xiuhui Zheng, Juncong Yuan, Qiuming He, De Chen, Chaohe Yang, and Xiang Feng*

Cite This: ACS Catal. 2025, 15, 14741–14750
Read Online

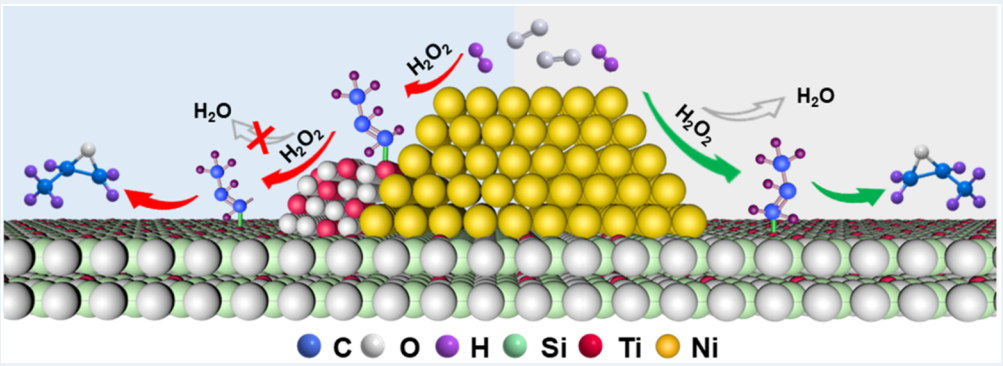

ABSTRACT: Direct propene epoxidation using H_2 and O_2 to produce propylene oxide (PO) is considered an environmentally friendly and revolutionary industrial process. With the necessity of finding alternatives to precious Au-based catalysts, there is a critical need for highly active nonprecious metal catalysts in epoxidation reactions. Herein, we successfully constructed different degrees of strong metal–support interaction (SMSI) by reversing TiO_2 islands into TiO_x layers over Ni nanoparticles in a H_2 atmosphere. The resulting nonprecious 1.27%Ni/Ti–SiO_2 catalyst with moderate SMSI exhibited a remarkable 90.6% selectivity toward PO with a formation rate of 9.23 $g_{PO}h^{-1}g_{Ni}^{-1}$. Mechanistic investigations revealed that tetrahedral-Ti sites and Ni–TiO_x overlayers synergistically catalyze propene epoxidation with H_2 and O_2. The Ni–TiO_x interface provided abundant unsaturated Ti (TiO_x) sites, enhancing the adsorption capacity of propene and consequently accelerating subsequent propene epoxidation with in situ synthesized H_2O_2. This study introduces an original approach for the utilization of nonprecious metal catalysts in gas-phase propene epoxidation, with promising implications for advancing industrial olefin epoxidation processes.

KEYWORDS: *propene epoxidation, Ni/Ti–SiO_2, SMSI, Ni–TiO_x interfaces, TiO_x layers*

1. INTRODUCTION

Propene oxide (PO) serves as a crucial chemical precursor extensively employed in the synthesis of poly(ether polyols), pesticide emulsifiers, nonionic surfactants, wetting agents, and flame retardants.[1−3] Traditional methods for producing PO include the chlorohydrin method and the co-oxidation method.[4,5] In comparison to traditional routes, direct propene epoxidation using H_2 and O_2 offers distinct advantages in terms of environmental friendliness, efficiency, and sustainability, rendering it a promising alternative. Since the groundbreaking work of Haruta et al.,[6] who demonstrated the high selectivity of PO using Au/TiO_2 catalysts in propene epoxidation with hydrogen and oxygen, significant advancements have been made in the development of Au–Ti catalysts. It is widely accepted that the H_2O_2 species are formed on the surface of Au nanoparticles (NPs) and then diffuse to the tetrahedral-Ti (TiO_4) sites to form Ti–OOH intermediates.[7−10] These intermediates undergo epoxidation reactions with propene adsorbed on the tetrahedral-Ti. Furthermore, non-noble-metal-based catalysts such as Ni, Co, and Cu offer greater economic efficiency and potential compared with noble metal catalysts like Au and Pd. Recent work by Zhao et al.[11] demonstrated the synthesis of a Ni_{2-x}P-VNi electrocatalyst with exceptional performance for H_2O_2 synthesis. Han et al.[12] reported the direct conversion of water to H_2O_2 on Ni catalyst surfaces, enabling the partial oxidation of propene to PO. Overall, Ni emerges as a promising non-noble metal catalyst for this epoxidation reaction.

Received: April 21, 2025
Revised: August 4, 2025
Accepted: August 4, 2025

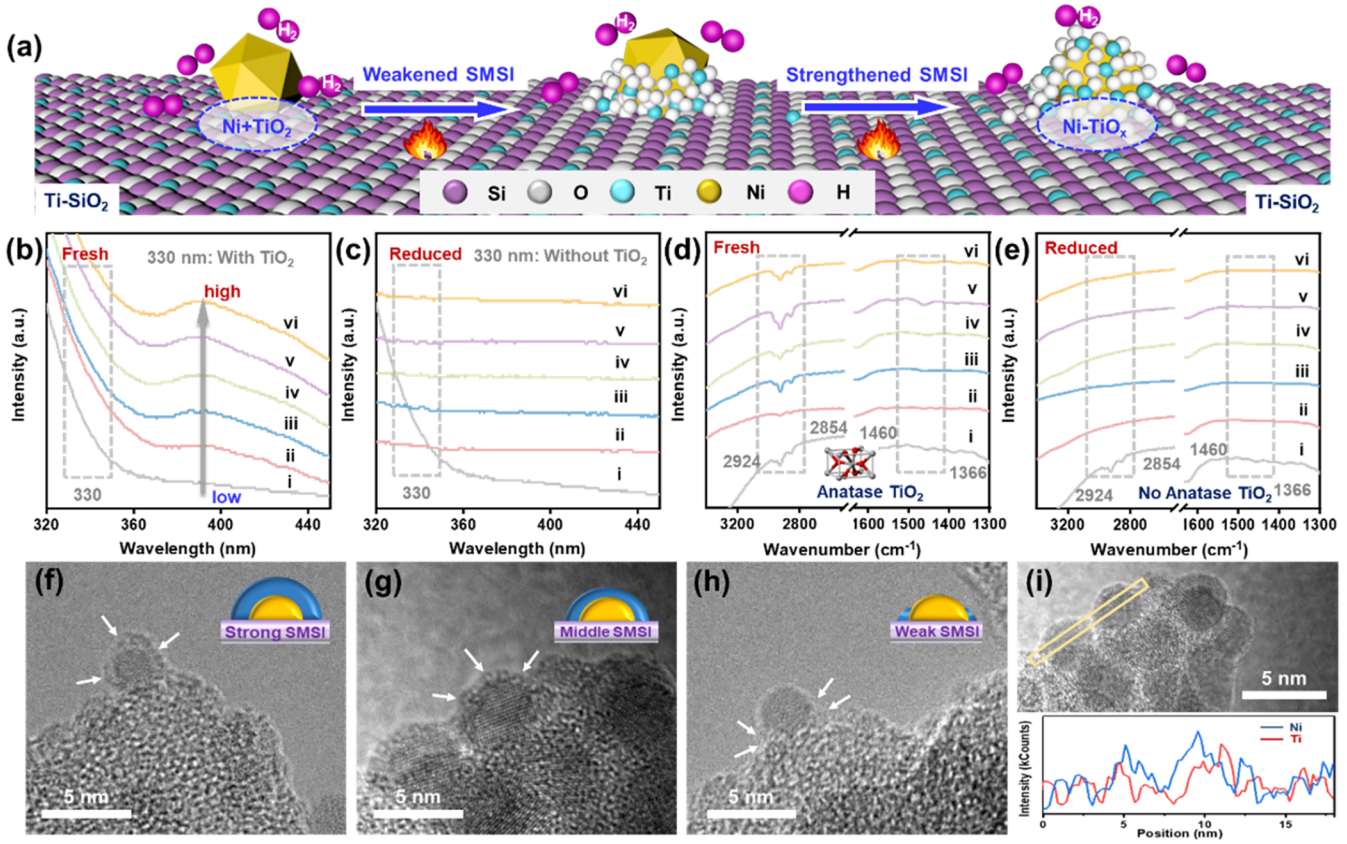

Figure 1. (a) Scheme showing Ti−SiO_2-supported Ni NPs catalysts with different metal−support interactions, UV−vis spectra of (b) fresh Ni/Ti−SiO_2 catalysts, and (c) reduced Ni/Ti−SiO_2 catalysts after reduction in hydrogen at 500 °C for 4 h. FTIR spectra of (d) fresh Ni/Ti−SiO_2 catalysts and (e) reduced Ni/Ti−SiO_2 catalysts after reduction in hydrogen at 500 °C for 4 h. (i) Ti−SiO_2, (ii) 0.47%Ni/Ti−SiO_2, (iii) 0.85%Ni/Ti−SiO_2, (iv) 1.10%Ni/Ti−SiO_2, (v) 1.27%Ni/Ti−SiO_2, and (vi) 1.54%Ni/Ti−SiO_2 catalysts. High-resolution transmission electron microscopy (HRTEM) images of (f) 0.47%Ni/Ti−SiO_2, (g) 1.27%Ni/Ti−SiO_2, and (h) 1.54%Ni/Ti−SiO_2 catalysts. Insets in parts f and h show models of different catalysts. The white arrows highlight the overlayers. (i) EDS line scans of Ni particles with overlayers for 1.27%Ni/Ti−SiO_2.

The concept of the strong metal support interaction (SMSI) is crucial in multiphase catalysis. On the one hand, the anchoring effect of the support on metal particles restricts their migration and aggregation, effectively preventing sintering and maintaining the high activity of the catalyst. On the other hand, the construction of SMSI is usually accompanied by the generation of interface structures, and the multiple interface active sites generated can optimize catalytic reaction performance.[13−16] This is mainly attributed to the Fermi level difference between the metal and the support, which leads to electron transfer and regulates the electronic state and coordination environment of metal atoms, resulting in distinct chemical adsorption and reaction toward reactants, products, and active intermediates.[13,17−19] Recent studies by Weckhuysen et al.[20] demonstrated the construction of various SMSI structures on Ni/TiO_2 catalysts through adjustment of the reduction temperature. Compared with the Ni/TiO_2 catalyst partially encapsulated by TiO_x, the Ni/TiO_2 catalyst completely covered by TiO_x exhibited a significant increase in C_{2+} selectivity during CO/CO_2 cohydrogenation reactions, because the abundant Ni−TiO_x interfaces boost C−C coupling reactions by providing a carbon species reservoir. Additionally, Ma et al.[21] modified the distorted TiO_{2-x} layer on Ni NP surfaces through SMSI, yielding a catalyst with abundant $Ni^{\delta-}/TiO_{2-x}$ interfaces. The strong binding between these $Ni^{\delta-}/TiO_{2-x}$ catalytic sites and carbon atoms inhibits methane generation and promotes C−C growth, thereby generating C_{2+} products on the Ni surface during Fischer−Tropsch synthesis. However, the application of SMSI was not reported in gas-phase epoxidation because the stable TS-1 support makes it difficult to construct SMSI in a reducing atmosphere.[22−24]

In this study, SMSI between Ni and TiO_x layers was constructed by co-reducing Ni and TiO_2 islands on the Ti−SiO_2 support, forming a Ni−TiO_x interface. Consequently, the Ni sites in Ni/Ti−SiO_2 are used for H_2O_2 synthesis between H_2 and O_2, and the tetra-coordinated Ti sites (TiO_4) in Ti−SiO_2 support are subsequently used to catalyze propene epoxidation with the in situ-generated H_2O_2 on Ni sites. The SMSI strengthens propene adsorption with electron-rich C═C bonds. The resultant 1.27%Ni/Ti−SiO_2 catalyst with SMSI exhibited remarkable PO selectivity of 90.6% and a PO formation rate of 9.23 $g_{PO}h^{-1}g_{Ni}^{-1}$ at 200 °C. This approach not only provides new insights into the strong metal−support interactions (SMSIs) by utilization of TiO_2 islands but also presents a nonprecious metal catalyst for direct propene epoxidation with H_2 and O_2.

2. RESULTS AND DISCUSSION

2.1. SMSI Constructed on Ni/Ti−SiO_2 Catalysts. Initially, a silica support doped with Ti (Ti−SiO_2) was prepared according to previous research.[25] Subsequently, various amounts of Ni were loaded onto the Ti−SiO_2 support by using the deposition−precipitation method. The resulting

https://doi.org/10.1021/acscatal.5c02681
ACS Catal. 2025, 15, 14741−14750

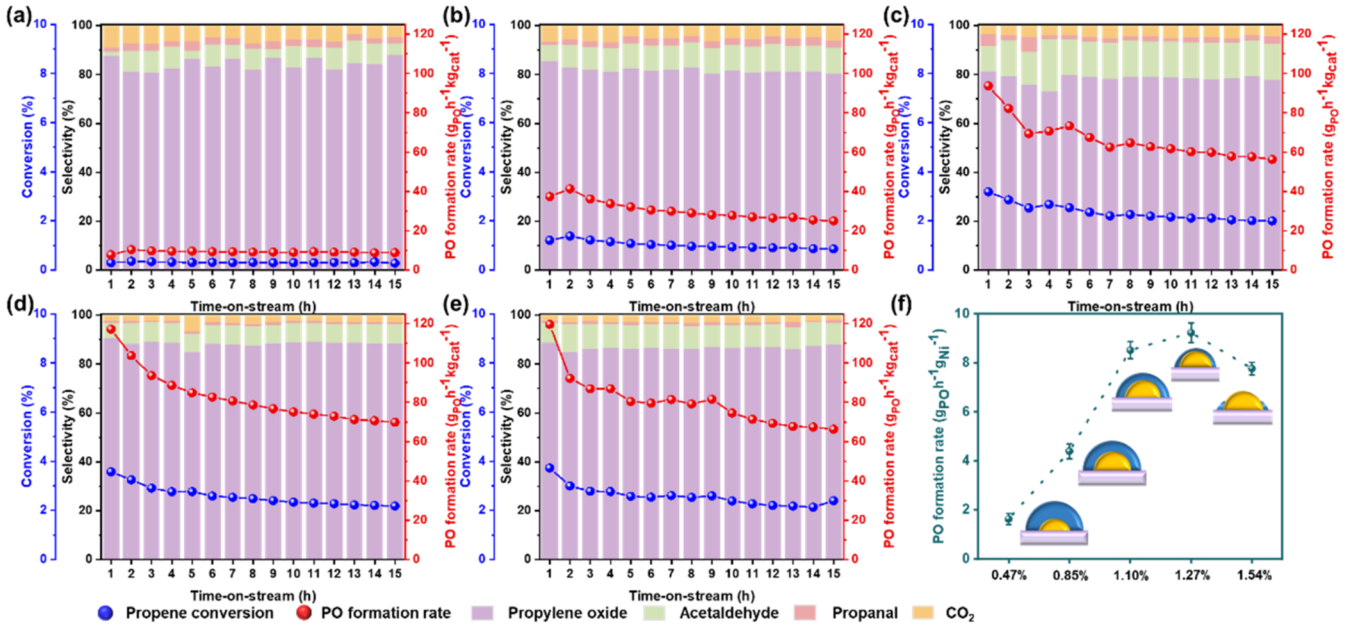

Figure 2. PO formation rate, propene conversion, and reaction selectivity of (a) 0.47%Ni/Ti−SiO_2, (b) 0.85%Ni/Ti−SiO_2, (c) 1.10%Ni/Ti−SiO_2, (d) 1.27%Ni/Ti−SiO_2, and (e) 1.54%Ni/Ti−SiO_2 catalysts (reduction in hydrogen at 500 °C for 4 h). (f) PO formation rates of different catalysts in units of $g_{PO}h^{-1}g_{Ni}^{-1}$. Reaction conditions: 0.15 g of the catalyst; feed gas with $H_2/O_2/C_3H_6/N_2$ = 1:1:1:7 (vol %); space velocity at 14 000 $mLg_{Cat}^{-1}h^{-1}$.

solid was then dried and reduced at high temperatures in a hydrogen atmosphere to produce a series of *x*% Ni/Ti−SiO_2 catalysts, where *x* represents the actual loading amount of the Ni metal determined by ICP analysis (Table S1). The powder X-ray diffraction patterns (XRD) of Ti−SiO_2 and Ni/Ti−SiO_2 did not exhibit characteristic peaks for Ni and Ti species (Figure S1). The absence of these peaks is attributed to the high dispersion and low content of Ni and Ti species,[26] as determined by the ICP-AES results (Table S1). The N_2 adsorption−desorption isotherms of the samples conformed to type-IV isotherms according to the IUPAC standard, suggesting the presence of mesoporous structures in the material (Figure S2a).[22] Pore-size distribution revealed that the majority of pores in both Ti−SiO_2 and Ni/Ti−SiO_2 samples fell within the range 7−11 nm, indicative of a typical mesoporous structure (Figure S2b). Based on the above results (Table S1), the specific surface area of the Ni/Ti−SiO_2 samples, loaded with varying amounts of the Ni metal, showed no significant differences compared with the parent Ti−SiO_2.

In UV−vis spectra of fresh Ti−SiO_2 (Figure S3), a strong electron transition signal peak typically appears around 206 nm, indicating the transition of 2p electron orbitals of framework oxygen to the empty d electron orbitals of Ti ions in the framework.[22] This observation not only confirms the presence of Ti into the framework but also suggests that the Ti is highly dispersed, forming isolated −Si−O−Ti−O−Si− units.[27] Additionally, the characteristic peak at 390 nm is attributed to hydrated nickel species ($Ni(OH)_2$ species), with an increase in peak intensity signaling a higher loading of nickel species.[28,29] A weak peak at 330 nm corresponds to the characteristic peak of anatase TiO_2, known to reduce the efficiency of epoxidation reactions involving the decomposition of hydrogen peroxide (H_2O_2).[30,31] After reduction, all Ni/Ti−SiO_2 catalysts exhibited a significant decrease in the peak at 330 nm, which is associated with the reduction or transformation of anatase TiO_2 species (Figure 1b,c).[32,33] Notably, the fresh catalyst showed characteristic peaks at 2924, 2854, 1460, and 1368 cm^{-1} in Fourier transform infrared (FTIR) spectra, indicative of anatase TiO_2 (Figure 1d).[34,35] After the catalyst underwent high-temperature reduction treatment, the intensity of the characteristic peaks associated with anatase TiO_2 in the reduced Ni/Ti−SiO_2 catalyst decreased, indicating a reduction in the anatase TiO_2 content, which aligned with the UV−vis results (Figure 1e). In addition, Figure S4a−d shows that the characteristic peak at 965 cm^{-1} attributed to Si−O−Ti species did not show significant changes in fresh and reduced catalysts. Subsequent analysis in Figures S5 and S6 revealed that the characteristic peak intensity of anatase TiO_2 in the used Ni/Ti−SiO_2 catalyst remained consistently negligible after reaction, suggesting the irreversibility of this change and the stability of the as-formed catalytic structure.

Integrating the UV−vis and FTIR results, it is deduced that the fresh catalyst contained a high proportion of tetra-coordinated Ti (TiO_4) along with a small quantity of anatase TiO_2. Subsequent high-temperature reduction treatment facilitated the transformation of TiO_2 islands to TiO_x species, which then migrated to the surface of Ni particles, constructing the typical SMSI (Figure 1a).

To confirm SMSI, TEM was used to analyze the Ni/Ti−SiO_2 samples. TEM images and particle-size distributions in Figure S7a−e showed that the Ni/Ti−SiO_2 catalysts with varying Ni loadings (0.47−1.57%) showed relatively uniform Ni nanoparticles of approximately 2−3 nm in size, across the series of samples, based on the calculation of approximately 150 particles from TEM images. The HRTEM images in Figure S7f provided confirmation of the presence of the Ni(111) crystal plane, exhibiting a lattice spacing of 0.202 nm.[36,37] Furthermore, the HRTEM image in Figure 1f illustrates that the Ni metal particles in the 0.47%Ni/Ti−SiO_2 sample were enveloped in an oxide coating, resembling the typical SMSIs.[20,38−40] The results from Figures 1f,g and S7−S10 clearly demonstrated that the Ni metal particles in the

https://doi.org/10.1021/acscatal.5c02681
ACS Catal. 2025, 15, 14741−14750

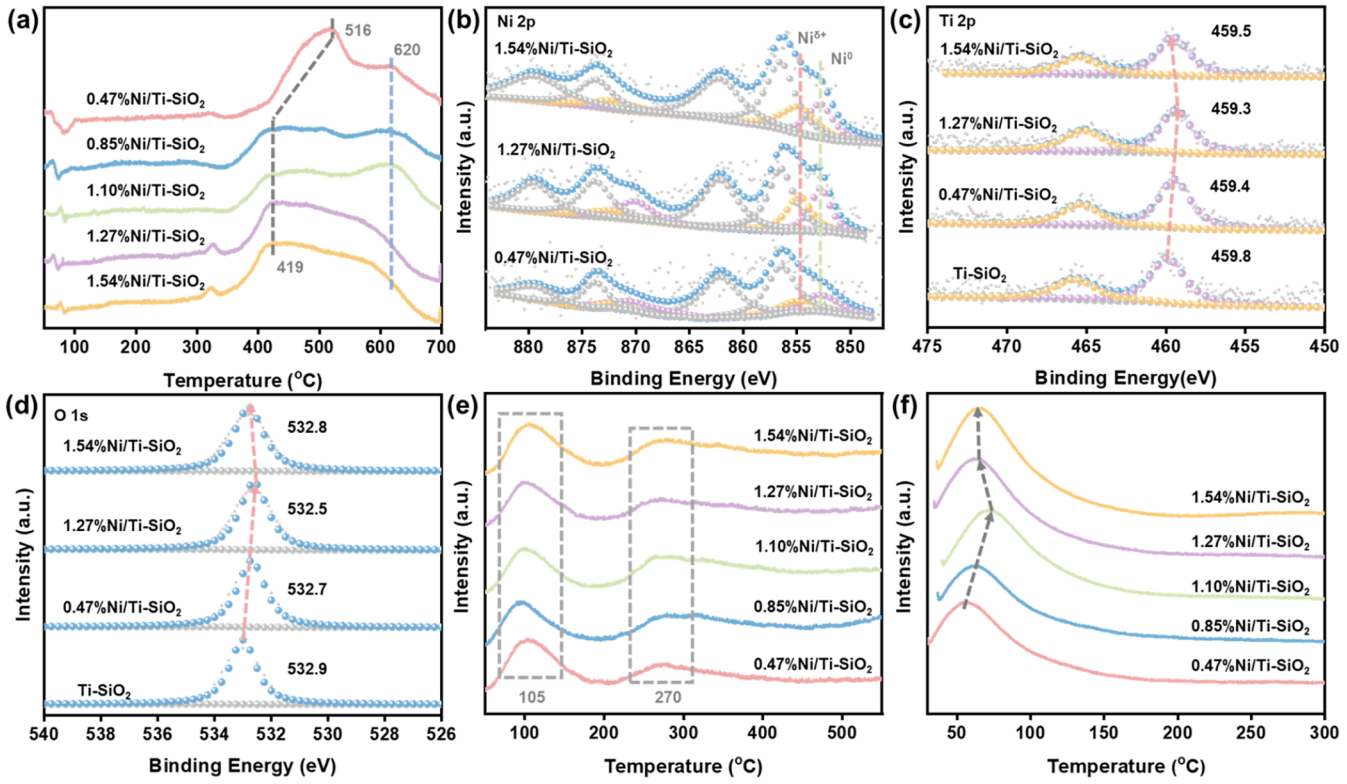

Figure 3. (a) H_2-TPR profiles of different Ni/Ti−SiO_2. (b) Ni 2p XPS spectra, (c) Ti 2p XPS spectra, and (d) O 1s XPS spectra for Ti−SiO_2 and Ni/Ti−SiO_2, (e) O_2-TPD profile of different Ni/Ti−SiO_2. (f) In situ adsorption−desorption experiment of propene on 0.47%Ni/Ti−SiO_2, 0.85% Ni/Ti−SiO_2, 1.10%Ni/Ti−SiO_2, 1.27%Ni/Ti−SiO_2, and 1.54%Ni/Ti−SiO_2 catalysts.

sample were encapsulated by an amorphous oxide coating rather than carbonaceous species. As the Ni content increased, the coating of TiO_x species with the same content gradually diminished, and the TiO_x layer became thinner.[41−45] Particularly, when the Ni content was high at 1.54%, the inadequate coating caused the exposed Ni metal nuclei, indicating weakened SMSI, as shown in Figure 1h. EDS line-scan results revealed a similar distribution trend of Ni and Ti species (Figure 1i), suggesting that the surface coating of Ni metal particles consists of TiO_x layers rather than TiO_2.[20,39] These findings suggest that after undergoing high-temperature reduction treatment, a series of Ni/Ti−SiO_2 samples with various SMSI were successfully constructed, resulting in the transformation of anatase TiO_2 into amorphous TiO_x.

2.2. Effect of SMSI for Propene Epoxidation with H_2 and O_2. For propene epoxidation with H_2 and O_2, the influence of internal and external diffusion was first eliminated (Figures S11 and S12). The reaction results from Table S3 indicated that the catalyst without Ni loading (SiO_2, TiO_2, and Ti−SiO_2) or Ti loading (Ni/SiO_2) was ineffective in propene epoxidation. However, the Ni/TiO_2 catalyst with both Ti and Ni sites also showed low PO selectivity (0.09%) due to the excessive hydrogenation of propene to propane (Figure S15). Moreover, the physical mixture of Ni/SiO_2 and Ti−SiO_2 exhibited a PO formation rate of 8.97 $g_{PO}h^{-1}kg_{Cat}^{-1}$ and PO selectivity of 55.25% (Table S3 Entry 7), potentially due to the spatial distance between the Ni and Ti active sites, which could restrain the effective H_2O_2 transfer from Ni sites to Ti sites.[46] In contrast, 1.27%Ni/Ti−SiO_2 catalysts with SMSI demonstrated higher activity and PO selectivity, reaching 117.21 $g_{PO}h^{-1}kg_{Cat}^{-1}$ and 90.64% (Table S3 Entry 8).[47−50] Furthermore, the effect of the Ni/Ti ratio on epoxidation performance was examined by maintaining a constant Ni content while varying the Ti content. As shown in Figure S16, a Ni/Ti ratio of 1.05 yields optimal epoxidation performance. These findings confirmed that gas-phase propene epoxidation necessitated the intimate interaction of Ni and tetra-coordinated Ti sites, and the adjacent Ni and Ti sites could boost the epoxidation reaction.

Specifically, the SMSI of Ni/Ti−SiO_2 catalysts was then regulated, and as the SMSI gradually weakened, the PO formation rate increased from 10.32 to 119.68 $g_{PO}h^{-1}kg_{Cat}^{-1}$ (Figure 2a−e), which was attributed to the increase in the number of Ni sites in Ni/Ti−SiO_2 catalysts. It is worth noting that all Ni catalysts exhibit varying degrees of deactivation during the reaction, which may be related to the coverage of active sites by carbon deposits (Figure S17). The main byproducts of all samples are acetaldehyde and acetaldehyde, indicating that the formed PO subsequently tends to undergo isomerization or cracking. Besides, propane and acrolein were not detected as byproducts of propylene epoxidation, which may be related to the promoting effect of SMSI. In order to compare performance on Ni/Ti−SiO_2 samples with various SMSIs, the highest PO formation rate per gram of Ni ($g_{PO}h^{-1}g_{Ni}^{-1}$) was calculated on various Ni catalysts. Figure 2f illustrates that with the construction of different SMSIs in Ni/Ti−SiO_2 catalysts, the PO formation rate of Ni catalysts followed a volcano-like trend, even at high Ni loading (Figure S18). In addition, the influence of SMSI on the epoxidation performance was further discussed by changing the reduction temperature. Additionally, the impact of SMSI on epoxidation performance was further investigated by varying the reduction temperature. As shown in Figure S19, an optimal SMSI effect can be achieved at 500 °C, enhancing the epoxidation activity.

https://doi.org/10.1021/acscatal.5c02681
ACS Catal. 2025, 15, 14741−14750

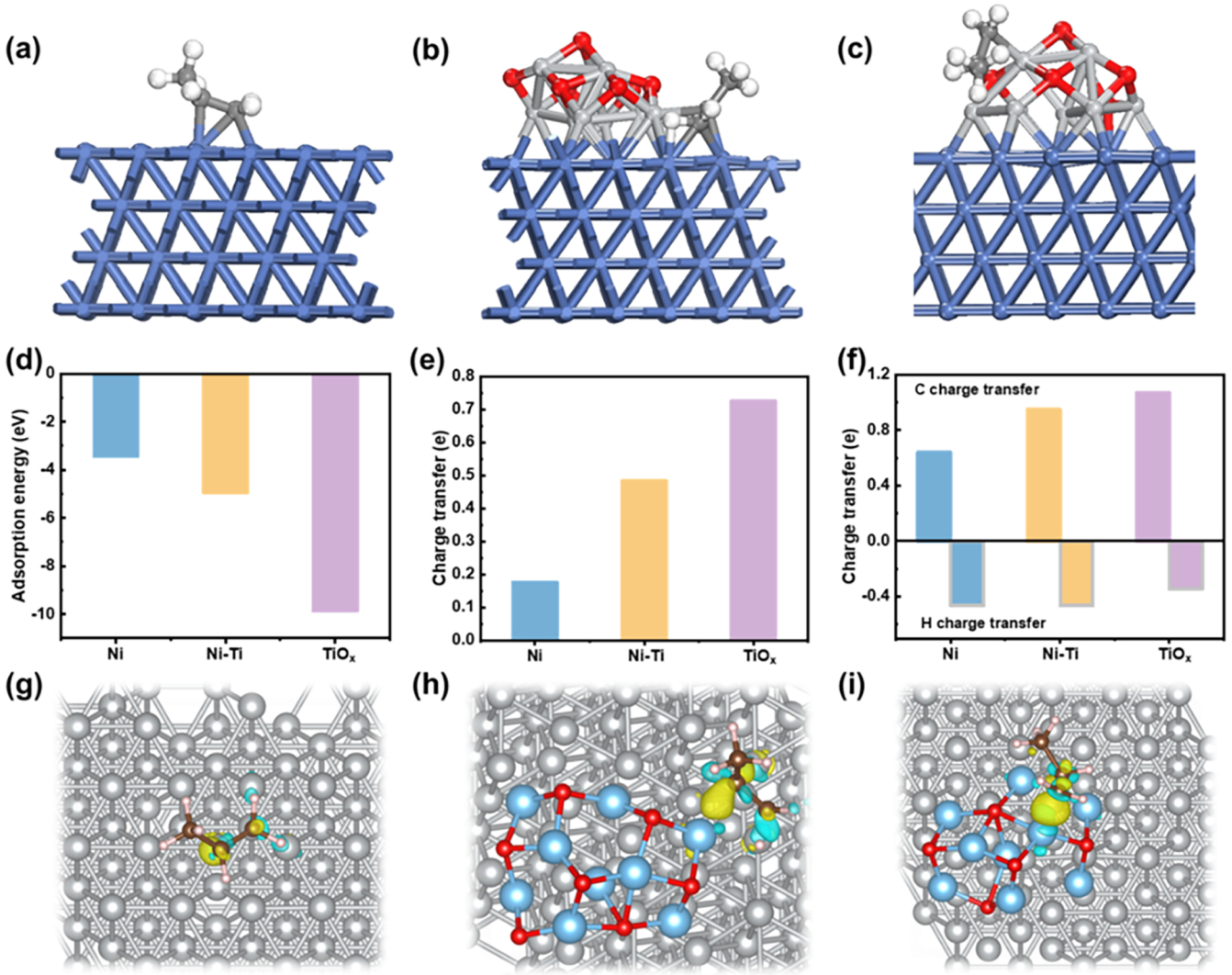

Figure 4. Optimized structures of C_3H_6 adsorbed on (a) Ni nanoparticles, (b) Ni−Ti interfaces of the TiO_x cluster on Ni nanoparticles, and (c) TiO_x cluster on Ni nanoparticles. (d) Adsorption energy, (e) charge transfer, and (f) partial charge transfer of C_3H_6 on Ni nanoparticles (Ni), Ni−Ti interfaces of the TiO_x cluster on Ni nanoparticles (Ni−Ti), and the TiO_x cluster on Ni nanoparticles (TiO_x). The differential charge density plots of C_3H_6 adsorbed on various surfaces of (g) Ni, (h) Ni−Ti, and (i) TiO_x. Light blue and yellow isosurfaces indicate a decrease and increase of 0.01 eV $Å^{-3}$, respectively.

Considering these samples with similar Ni nanoparticles (2−3 nm) and Ti−SiO_2 supports (Figure S7a−e), the effect of metal particle size can be excluded; thus, the differences in performance ($g_{PO}h^{-1}g_{Ni}^{-1}$) were attributed to the distinct SMSI in the aforementioned Ni/Ti−SiO_2 catalysts. Figure S20 presents a linear relationship between the H_2 consumption and the Ni loading in Ni/Ti−SiO_2 catalysts with varying SMSIs, proving that Ni particles were active sites for producing H_2O_2 from H_2 and O_2. Besides, the synthesis experiments of H_2O_2 from H_2/O_2 were conducted on various samples. Figure S21 shows a linear relationship between the H_2O_2 formation rate and Ni content, further confirming the in situ production of H_2O_2 from H_2/O_2 at Ni sites. Interestingly, the catalysts with the SMSI, such as the 0.47%Ni/Ti−SiO_2 samples, exhibited higher H_2 efficiency, while those with weaker MSI showed lower H_2 efficiency (Figure S22). The change in H_2 efficiency can be attributed to the difference in SMSI on the Ni/Ti−SiO_2 catalyst. Specifically, H_2O_2 decomposition experiments on Ni/Ti−SiO_2 with and without SMSI were compared. The results in Table S4 suggest that the presence of SMSI provided an excellent Ni−TiO_x interface, which was beneficial for stabilizing H_2O_2 (H_2O_2 decomposition of 3.23%), while the absence of SMSI led to decomposition of H_2O_2 (H_2O_2 decomposition of 4.98%).[6,50] The above phenomenon indicated that by constructing SMSI between Ni and TiO_2 in the Ti−SiO_2 support, the reversed TiO_x can weaken the decomposition of H_2O_2 intermediates. Therefore, it was reasonable for Ni catalysts with the strongest MSI to demonstrate higher H_2 efficiency.[51] To sum up, the above phenomenon suggested that an appropriate SMSI in the catalyst can effectively boost the propene epoxidation using H_2 and O_2.

2.3. Promotion Mechanism by Varying Degrees of SMSI. Hydrogen programmed temperature reduction (H_2-TPR) is often used to investigate SMSIs. Specifically, samples with low Ni loading (0.47%Ni) showed distinct H_2 consumption peaks at 516 and 620 °C, corresponding to the reduction of NiO species with weak and strong interactions with the support.[52,53] The reduction peak (516 °C) shifted toward a lower temperature (419 °C), proving a weakened

https://doi.org/10.1021/acscatal.5c02681
ACS Catal. 2025, 15, 14741−14750

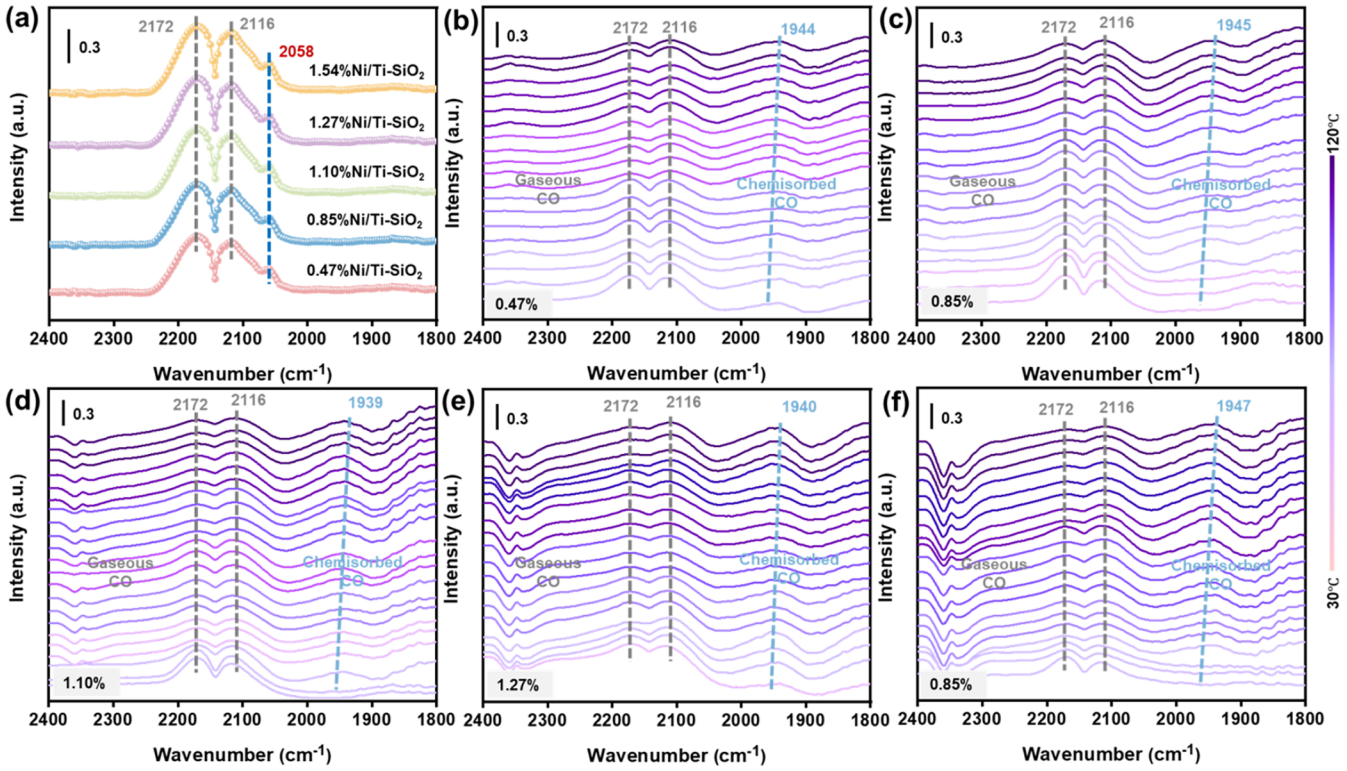

Figure 5. (a) In situ CO-DRIFTS spectra of Ni/Ti−SiO_2 catalysts at room temperature. In situ CO-DRIFTS spectra of (b) 0.47%Ni/Ti−SiO_2, (c) 0.85%Ni/Ti−SiO_2, (d) 1.10%Ni/Ti−SiO_2, (e) 1.27%Ni/Ti−SiO_2, and (f) 1.54%Ni/Ti−SiO_2 catalysts under programmed heating at 30−120 °C. The corresponding spectra were recorded in 2400−1800 cm^{-1} at different temperatures with the time stream on.

interaction between NiO species and the support. Besides, the intensity of the peak at 620 °C decreased, indicating the reduction in SMSI between NiO species and the support (Figure 3a). Overall, the SMSI gradually weakened with the increase in Ni loading, which agreed well with TEM analysis (Figure 1f−h). XPS analysis of Ni/Ti−SiO_2 catalysts (Figure 3b−d) further elucidated the electronic structure variances resulting from different SMSIs. According to Figure 3b, binding energy peaks were observed at 852.8, 854.8, 856.5, and 862.2 eV, corresponding to metal Ni^0, $Ni^{\delta+}$, and two satellite peaks, respectively.[51] As the Ni loading increased, the proportion of $Ni^{\delta+}$ species first increased from 42.9 to 49.5% and then decreased to 47.2% (Table S5), indicating a fluctuation in the number of electrons lost by Ni species. Figure 3c illustrates a contradictory trend in the electronic structure changes of Ti species. As SMSI weakened, the binding energy of Ti 2p initially shifted to lower-energy bands and subsequently increased, remaining lower than the binding energy of Ti in the parent Ti−SiO_2. This indicated that the number of electrons obtained by Ti species in different SMSIs first increased and then decreased, and Ti in all Ni/Ti−SiO_2 samples has obtained partial electrons, which could be from Ni sites due to SMSI interactions. The electronic variation trend of the O 1s species in Figure 3d closely mirrored that of Ti 2p. In Figure 3e, the O_2-TPD results of samples with different SMSIs show that the desorption peak in the low temperature (∼100 °C) is related to the physically adsorbed O_2 species, while the peak in the high temperature (∼270 °C) is related to the chemically adsorbed O species (O_2^{2-}, O_2^-).[54] The O_2 desorption peaks across all samples with various SMSIs exhibited similar curves and intensities, suggesting comparable adsorption and activation capabilities of the corresponding O_2. Figure 3f and Table S6 illustrate the pulse propene adsorption results of different catalysts. With SMSI, the propene adsorption was enhanced compared with the sample without SMSI (Figure S23). The decrease in the reaction order of propene in Figure S24 indicates that SMSI can strengthen propene adsorption, further supporting the above conclusion. Previous research indicated that propene adsorption relied on electron-rich C═C bonds binding to metal sites.[55,56] The electron-deficient species in SMSI likely enhanced the electron attraction to the C═C bond of propene, consistent with the XPS results (Figure 3b−d). Therefore, it was speculated that the exceptional SMSI structure (Ni−TiO_x) of the Ni/Ti−SiO_2 sample generated additional interfacial sites, thereby boosting propene adsorption capacity. In addition, as the SMSI weakened, the desorption peak initially shifted to higher temperatures and then subsequently to lower temperatures. Notably, the 1.27%Ni/Ti−SiO_2 samples with appropriate SMSI exhibited a suitable adsorption capacity of propene. Overall, changes in the TiO_x coating layer resulted in distinct interactions between Ni sites and the support, impacting electron transfer, active site formation, and adsorption behavior, consequently influencing catalytic performance.

To sum up, the Ni sites in the Ni−TiO_x interface catalyzed the generation of H_2O_2 intermediates from H_2 and O_2, and the SMSI constructed between Ni and TiO_2 reduced H_2O_2 decomposition and improved H_2 efficiency. In addition, the Ni−TiO_x interface in SMSI enhanced the adsorption of propene to boost the epoxidation reaction between adsorbed propene and in situ-generated H_2O_2.

The above results show that SMSI (Ni−TiO_x) enhances propene adsorption. However, the actual adsorption sites of propene cannot be further identified. Density functional theory

https://doi.org/10.1021/acscatal.5c02681
ACS Catal. 2025, 15, 14741−14750

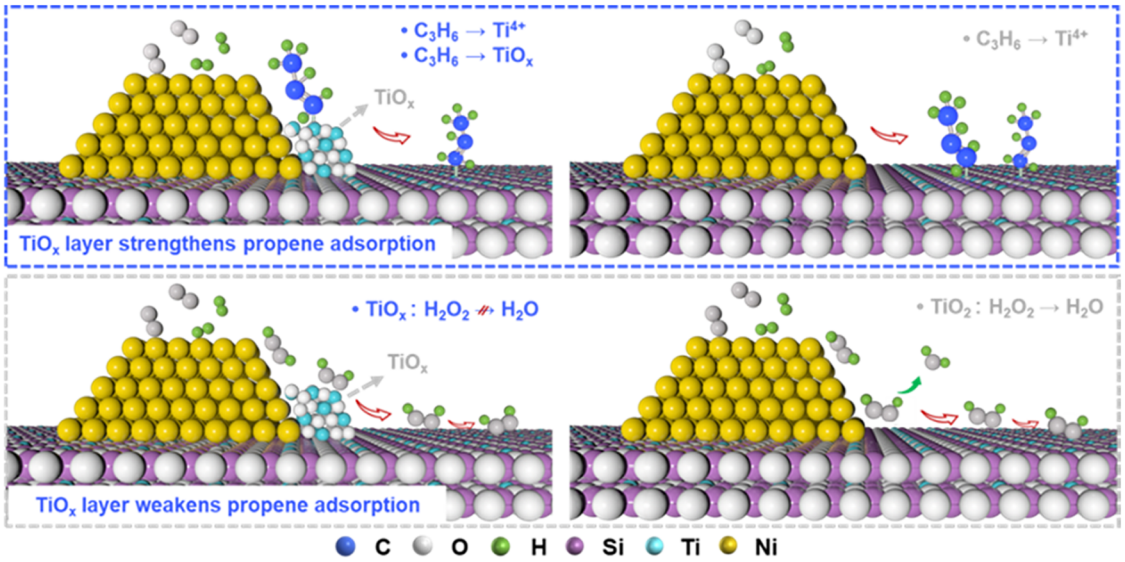

Figure 6. Scheme showing the strategy for boosting the propene epoxidation reaction via SMSI on the Ni/Ti−SiO_2 catalyst.

is employed to investigate the adsorption of C_3H_6 on the Ni/Ti−SiO_2 catalyst. The adsorption structure of C_3H_6 on Ni nanoparticles (Figure 4a), Ni−Ti interfaces of SMSI (Figure 4b), and TiO_x layers (Figure 4c) was first optimized. It was found that the propene adsorbed on TiO_x layers showed the lowest adsorption energy (−9.86 eV), as shown in Figure 4d, lower than the adsorption energy on Ni nanoparticles alone (−3.42 eV) and Ni−Ti interfaces (−4.94 eV). The significantly enhanced C_3H_6 adsorption on TiO_x clusters was attributed to the optimized structures of TiO_x clusters on Ni nanoparticles due to the introduction of a reducible C_3H_6 atmosphere. Moreover, the charge transfer of adsorbed C_3H_6 followed the order (TiO_x: 0.725 > Ni−Ti: 0.484 > Ni: 0.176) as shown in Figure 4e, which correlated with the adsorption energies. Figure 4f suggests that the electron gained by propene was attributed to the interactions between the carbon atoms and Ni/Ti species. The differential charge density plots in Figure 4g−i further demonstrated the above conclusion. The above results indicated that propene can adsorb on TiO_x layers on Ni nanoparticles in Ni−Ti interfaces formed by SMSI, resulting in strong electron transfer between TiO_x clusters and propene. These results showed that the adsorption of propene can be effectively enhanced by constructing the SMSI on Ni nanoparticles covered by TiO_x layers.

The structure of Ni−TiO_x was further probed by in situ CO-DRIFTS spectra. Figure 5a illustrates that the infrared adsorption peaks at 2172 and 2116 cm^{-1} for gaseous CO adsorption and a peak at 2058 cm^{-1} for CO species linearly adsorbed on the Ni^0 site.[20,57,58] During the N_2 purging process at 30−120 °C, the broadband between 1900 and 2000 cm^{-1} indicates that CO undergoes bridge adsorption at interface sites such as $Ni^{\delta+}$. It should be noted that there is no linear CO adsorption peak at the Ni^0 site, indicating that electron-deficient ($Ni^{\delta+}$) species have a stronger adsorption ability for CO at high temperatures. The SMSI at the Ni−TiO_x interface led to a partial positive charge on Ni and partial negative charges on Ti and O atoms, attributed to the electron-withdrawing effect of the O and Ti atoms. Varied bands at 1947−1938 cm^{-1} signified differences in CO adsorption ability among these samples (Figure 5b−f). The position of the vibration peaks initially decreased and then increased with the change of SMSI, indicating that the CO adsorption capacity initially strengthened and then weakened. The above results indicated that catalysts with appropriate SMSI exhibited good adsorption capacity for CO. Therefore, the 1.27%Ni/Ti−SiO_2 sample had moderate SMSI, resulting in propene adsorption ability and thus excellent PO performance, which was attributed to the presence of Ni−TiO_x interfaces generated by SMSI.

The promoting mechanism of SMSI on the Ni/Ti−SiO_2 catalyst for the propene epoxidation reaction was proposed, as illustrated in Figure 6. In terms of the principle of SMSI, SMSI was successfully constructed through high-temperature reduction treatment, resulting in the formation of an abundant Ni−TiO_x interface. The presence of the Ni−TiO_x interface inhibited the ineffective decomposition of H_2O_2 generated in situ from H_2 and O_2 over Ni sites. In addition, the results showed that the Ni−TiO_x interface further enhanced the epoxidation reaction because SMSI could promote electron transfer, resulting in the generation of electron-deficient interface sites. These TiO_x species could further boost the adsorption capacity of propene. The Ni−TiO_x interface increased with an increase of Ni sites. However, the insufficient TiO_x species inhibited the formation of SMSI at a high Ni loading, resulting in a decrease in the Ni−TiO_x interface. Therefore, Ni/Ti−SiO_2 catalysts with appropriate SMSI exhibited a good adsorption capacity for propene, thereby boosting PO formation. In summary, H_2 and O_2 were converted into H_2O_2 over Ni sites and then reacted with propene adsorbed on the tetra-coordinated Ti (TiO_4), similar to the reaction pathway on the Au−Ti system.[47,49,50,59] The proximal TiO_x at the Ni−TiO_x interface was conducive to the adsorption of propene and the inhibition of H_2O_2 decomposition, further improving the epoxidation reaction. The above results indicate that the designed Ni−Ti catalyst (Ni/Ti−SiO_2) exhibits excellent propene epoxidation performance and has the potential to substitute for Au−Ti-based catalysts.

3. CONCLUSIONS

In this study, different SMSIs were successfully constructed between Ni and TiO_2 in Ni/Ti−SiO_2 catalysts through a high-temperature reduction treatment. TiO_2 in the Ti−SiO_2 support

https://doi.org/10.1021/acscatal.5c02681
ACS Catal. 2025, 15, 14741−14750

was successfully reduced to TiO_x species at the interface of Ni, forming SMSI of Ni−TiO_x and synergistically catalyzed propene epoxidation with Ti−SiO_2. The Ni/Ti−SiO_2 catalysts exhibited a PO generation rate of 9.23 $g_{PO}h^{-1}g_{Ni}^{-1}$ with 90.6% PO selectivity. The mechanism results revealed that TiO_x transformed from TiO_2 species effectively weakens the ineffective decomposition of H_2O_2 species and further strengthens propene adsorption, leading to enhanced PO formation. The strategy expands the design of novel catalysts for olefin epoxidation reactions.

■ ASSOCIATED CONTENT

Supporting Information

The Supporting Information is available free of charge at https://pubs.acs.org/doi/10.1021/acscatal.5c02681.

XRD patterns, N_2 adsorption−desorption isotherms and pore-size distribution plots, UV−vis spectra, FTIR spectra, TEM images, TGA, DTG curves of various supports and Ni catalysts, schematic diagram of the experimental apparatus, influences of mass diffusion, epoxidation performance of compared catalysts, relationship curve between Ni content and H_2 conversion/H_2O_2 formation, H_2 efficiency on various Ni catalysts, and C_3H_6 reaction orders of Ni catalysts (PDF)

■ AUTHOR INFORMATION

Corresponding Authors

Dong Lin − *Max Planck-Cardiff Centre on the Fundamentals of Heterogeneous Catalysis FUNCAT, Cardiff Catalysis Institute, School of Chemistry, Cardiff University, Cardiff CF24 4HQ, U.K.;* orcid.org/0000-0001-5313-8204; Email: LinD6@cardiff.ac.uk

Xiang Feng − *State Key Laboratory of Heavy Oil Processing, China University of Petroleum, Qingdao 266580, China;* orcid.org/0000-0001-7299-5690; Email: xiangfeng@upc.edu.cn

Authors

Defu Yin − *State Key Laboratory of Heavy Oil Processing, China University of Petroleum, Qingdao 266580, China*

Xiuhui Zheng − *State Key Laboratory of Heavy Oil Processing, China University of Petroleum, Qingdao 266580, China*

Juncong Yuan − *State Key Laboratory of Heavy Oil Processing, China University of Petroleum, Qingdao 266580, China*

Qiuming He − *State Key Laboratory of Heavy Oil Processing, China University of Petroleum, Qingdao 266580, China*

De Chen − *Department of Chemical Engineering, Norwegian University of Science and Technology, Trondheim 7491, Norway*

Chaohe Yang − *State Key Laboratory of Heavy Oil Processing, China University of Petroleum, Qingdao 266580, China;* orcid.org/0000-0001-6995-9170

Complete contact information is available at: https://pubs.acs.org/10.1021/acscatal.5c02681

Notes

The authors declare no competing financial interest.

■ ACKNOWLEDGMENTS

This work was supported by the National Natural Science Foundation of China-Outstanding Youth Foundation (No. 22322814) and National Natural Science Foundation of China (Nos. 22108307 and 22108305). D.L. gratefully acknowledges Cardiff University and the Max Planck Centre for Fundamental Heterogeneous Catalysis (FUNCAT) for financial support.

■ REFERENCES

(1) Ainsworth, S. J. Market for Polypropylene Is Strengthening as Economy Improves. *Chem. Eng. News Archive* **1992**, *70* (24), 9−11.

(2) Kim, I.; Ahn, J.-T.; Ha, C. S.; Yang, C. S.; Park, I. Polymerization of propylene oxide by using double metal cyanide catalysts and the application to polyurethane elastomer. *Polymer* **2003**, *44*, 3417−3428.

(3) Russo, V.; Tesser, R.; Santacesaria, E.; Di Serio, M. Chemical and Technical Aspects of Propene Oxide Production via Hydrogen Peroxide (HPPO Process). *Ind. Eng. Chem. Res.* **2013**, *52*, 1168−1178.

(4) Lu, J.; Luo, M.; Lei, H.; Li, C. Epoxidation of propylene on NaCl-modified silver catalysts with air as the oxidant. *Appl. Catal., A* **2002**, *237*, 11−19.

(5) Nijhuis, T. A.; Makkee, M.; Moulijn, J. A.; Weckhuysen, B. M. The Production of Propene Oxide: Catalytic Processes and Recent Developments. *Ind. Eng. Chem. Res.* **2006**, *45*, 3447−3459.

(6) Hayashi, T.; Tanaka, K.; Haruta, M. Selective Vapor-Phase Epoxidation of Propylene over Au/TiO_2 Catalysts in the Presence of Oxygen and Hydrogen. *J. Catal.* **1998**, *178*, 566−575.

(7) Feng, X.; Liu, Y.; Li, Y.; Yang, C.; Zhang, Z.; Duan, X.; Zhou, X.; Chen, D. Au/TS-1 catalyst for propene epoxidation with H_2/O_2: A novel strategy to enhance stability by tuning charging sequence. *AIChE J.* **2016**, *62*, 3963−3972.

(8) Lin, D.; Zheng, X.; Feng, X.; Sheng, N.; Song, Z.; Liu, Y.; Chen, X.; Cai, Z.; Chen, D.; Yang, C. Enhancing the dynamic electron transfer of Au species on wormhole-like TS-1 for boosting propene epoxidation performance with H_2 and O_2. *Green Energy Environ.* **2020**, *5*, 433−443.

(9) Lin, D.; Xu, Y.; Zheng, X.; Sheng, W.; Liu, Z.; Yan, Y.; Cao, Y.; Liu, Y.; Feng, X.; Chen, D.; Yang, C. Engineering sodium-decorated bifunctional Au-Ti sites to boost molecular transfer for propene epoxidation with H_2 and O_2. *AIChE J.* **2023**, *69*, e17999.

(10) Lin, D.; Zhang, Q.; Qin, Z.; Li, Q.; Feng, X.; Song, Z.; Cai, Z.; Liu, Y.; Chen, X.; Chen, D.; Mintova, S.; Yang, C. Reversing Titanium Oligomer Formation towards High-Efficiency and Green Synthesis of Titanium-Containing Molecular Sieves. *Angew. Chem., Int. Ed.* **2021**, *60*, 3443−3448.

(11) Zhou, Z.; Kong, Y.; Tan, H.; Huang, Q.; Wang, C.; Pei, Z.; Wang, H.; Liu, Y.; Wang, Y.; Li, S.; Liao, X.; Yan, W.; Zhao, S. Cation-Vacancy-Enriched Nickel Phosphide for Efficient Electrosynthesis of Hydrogen Peroxides. *Adv. Mater.* **2022**, *34*, 2106541.

(12) Xu, R.; Huang, H.; Wang, W.; Ding, L.; Lin, Q.; Li, J.; Zhang, Y.; Han, Y.; Wang, J.; Lu, X. Direct conversion of water to hydrogen peroxide on single electrode towards partial oxidation of propylene. *Chem. Eng. J.* **2023**, *461*, 141748.

(13) Li, D.; Li, X.; Gong, J. Catalytic Reforming of Oxygenates: State of the Art and Future Prospects. *Chem. Rev.* **2016**, *116*, 11529−11653.

(14) Lai, W. H.; Miao, Z.; Wang, Y. X.; Wang, J. Z.; Chou, S. L. Atomic-Local Environments of Single-Atom Catalysts: Synthesis, Electronic Structure, and Activity. *Adv. Energy Mater.* **2019**, *9*, 1900722.

(15) Pei, C.; Chen, S.; Fu, D.; Zhao, Z.-J.; Gong, J. Structured Catalysts and Catalytic Processes: Transport and Reaction Perspectives. *Chem. Rev.* **2024**, *124*, 2955−3012.

(16) Gao, C.; Lyu, F.; Yin, Y. Encapsulated Metal Nanoparticles for Catalysis. *Chem. Rev.* **2021**, *121*, 834−881.

(17) Pu, T.; Zhang, W.; Zhu, M. Engineering Heterogeneous Catalysis with Strong Metal−Support Interactions: Characterization, Theory and Manipulation. *Angew. Chem., Int. Ed.* **2022**, *62* (4), No. e202212278.

(18) Yang, J.; Li, W.; Wang, D.; Li, Y. Electronic Metal−Support Interaction of Single-Atom Catalysts and Applications in Electrocatalysis. *Adv. Mater.* **2020**, *32*, 2003300.
(19) van Deelen, T. W.; Hernández Mejía, C.; de Jong, K. P. Control of metal-support interactions in heterogeneous catalysts to enhance activity and selectivity. *Nat. Catal.* **2019**, *2*, 955−970.
(20) Monai, M.; Jenkinson, K.; Melcherts, A. E. M.; Louwen, J. N.; Irmak, E. A.; Van Aert, S.; Altantzis, T.; Vogt, C.; van der Stam, W.; Duchoň, T.; Šmíd, B.; Groeneveld, E.; Berben, P.; Bals, S.; Weckhuysen, B. M. Restructuring of titanium oxide overlayers over nickel nanoparticles during catalysis. *Science* **2023**, *380*, 644−651.
(21) Xu, M.; Qin, X.; Xu, Y.; Zhang, X.; Zheng, L.; Liu, J.-X.; Wang, M.; Liu, X.; Ma, D. Boosting CO hydrogenation towards C_{2+} hydrocarbons over interfacial TiO_{2-x}/Ni catalysts. *Nat. Commun.* **2022**, *13*, No. 6720.
(22) Guo, Y.; Zhang, Z.; Xu, J.; Duan, X.; Zhou, X. Suppression of TS-1 Aggregation by Freeze-Drying to Enhance Au Dispersion for Propylene Epoxidation Using H_2 and O_2. *Ind. Eng. Chem. Res.* **2023**, *62*, 8654−8664.
(23) Chen, L. H.; Li, X. Y.; Tian, G.; Li, Y.; Rooke, J. C.; Zhu, G. S.; Qiu, S. L.; Yang, X. Y.; Su, B. L. Highly Stable and Reusable Multimodal Zeolite TS-1 Based Catalysts with Hierarchically Interconnected Three-Level Micro−Meso−Macroporous Structure. *Angew. Chem., Int. Ed.* **2011**, *50*, 11156−11161.
(24) Zhang, W.; Xin, H.; Zhang, Y.; Jin, X.; Wu, P.; Xie, W.; Li, X. Bimetallic Pt-Fe catalysts supported on mesoporous TS-1 microspheres for the liquid-phase selective hydrogenation of cinnamaldehyde. *J. Catal.* **2021**, *395*, 375−386.
(25) Sinha, A. K.; Seelan, S.; Tsubota, S.; Haruta, M. A Three-Dimensional Mesoporous Titanosilicate Support for Gold Nanoparticles: Vapor-Phase Epoxidation of Propene with High Conversion. *Angew. Chem., Int. Ed.* **2004**, *43*, 1546−1548.
(26) Luo, M.; Ma, J.; Lu, J.; Song, Y.; Wang, Y. High-surface area CuO−CeO_2 catalysts prepared by a surfactant-templated method for low-temperature CO oxidation. *J. Catal.* **2007**, *246*, 52−59.
(27) Lin, D.; Feng, X.; Zheng, X.; Xu, Y.; Zhao, H.; Song, Z.; Wang, L.; Shan, H.; Xiao, F. S.; Chen, D.; Yang, C. Dimensional Regulation of Titanosilicate by Kinetically Controlled Intergrowth Crystals. *Adv. Funct. Mater.* **2023**, *33*, 2301179.
(28) Kukovecz, Á.; Kónya, Z.; Mönter, D.; Reschetilowski, W.; Kiricsi, I. UV−VIS investigations on Co, Fe and Ni incorporated into sol−gel SiO_2−TiO_2 matrices. *J. Mol. Struct.* **2001**, *563*−*564*, 403−407.
(29) Xiong, Z.; Lei, H.; Yang, J.; Liu, Y.; Gao, Z.; Li, Y.; Hao, C.; Wang, J. Deep-ultraviolet plasmon resonance of Ni nanoparticles embedded in $BaTiO_3$ matrix. *J. Alloys Compd.* **2022**, *924*, 166562.
(30) Khomane, R. B.; Kulkarni, B. D.; Paraskar, A.; Sainkar, S. R. Synthesis, characterization and catalytic performance of titanium silicalite-1 prepared in micellar media. *Mater. Chem. Phys.* **2002**, *76*, 99−103.
(31) Duprey, E.; Beaunier, P.; Springuel-Huet, M. A.; Bozon-Verduraz, F.; Fraissard, J.; Manoli, J. M.; Brégeault, J. M. Characterization of Catalysts Based on Titanium Silicalite, TS-1, by Physicochemical Techniques. *J. Catal.* **1997**, *165*, 22−32.
(32) Feng, X.; Duan, X.; Cheng, H.; Qian, G.; Chen, D.; Yuan, W.; Zhou, X. Au/TS-1 catalyst prepared by deposition−precipitation method for propene epoxidation with H_2/O_2: Insights into the effects of slurry aging time and Si/Ti molar ratio. *J. Catal.* **2015**, *325*, 128−135.
(33) Bordiga, S.; Damin, A.; Berlier, G.; Bonino, F.; Ricchiardi, G.; Zecchina, A.; Lamberti, C. The Role of Isolated Sites in Heterogeneous Catalysis: Characterization and Modeling. *Int. J. Mol. Sci.* **2001**, *2*, 167−182.
(34) Mino, L.; Spoto, G.; Ferrari, A. M. CO_2 Capture by TiO_2 Anatase Surfaces: A Combined DFT and FTIR Study. *J. Phys. Chem. C* **2014**, *118*, 25016−25026.
(35) Sui, R.; Rizkalla, A. S.; Charpentier, P. A. FTIR Study on the Formation of TiO_2 Nanostructures in Supercritical CO_2. *J. Phys. Chem. B* **2006**, *110*, 16212−16218.
(36) Wang, J.; Xin, S.; Xiao, Y.; Zhang, Z.; Li, Z.; Zhang, W.; Li, C.; Bao, R.; Peng, J.; Yi, J.; Chou, S. Manipulating the Water Dissociation Electrocatalytic Sites of Bimetallic Nickel-Based Alloys for Highly Efficient Alkaline Hydrogen Evolution. *Angew. Chem., Int. Ed.* **2022**, *61*, e202202518.
(37) Jia, X.; Zhang, X.; Rui, N.; Hu, X.; Liu, C.-j. Structural effect of Ni/ZrO_2 catalyst on CO_2 methanation with enhanced activity. *Appl. Catal., B* **2019**, *244*, 159−169.
(38) Zhang, Y.; Liu, J. X.; Qian, K.; Jia, A.; Li, D.; Shi, L.; Hu, J.; Zhu, J.; Huang, W. Structure Sensitivity of Au-TiO_2 Strong Metal−Support Interactions. *Angew. Chem., Int. Ed.* **2021**, *60*, 12074−12081.
(39) Frey, H.; Beck, A.; Huang, X.; van Bokhoven, J. A.; Willinger, M. G. Dynamic interplay between metal nanoparticles and oxide support under redox conditions. *Science* **2022**, *376*, 982−987.
(40) Dong, J.; Fu, Q.; Li, H.; Xiao, J.; Yang, B.; Zhang, B.; Bai, Y.; Song, T.; Zhang, R.; Gao, L.; Cai, J.; Zhang, H.; Liu, Z.; Bao, X. Reaction-Induced Strong Metal−Support Interactions between Metals and Inert Boron Nitride Nanosheets. *J. Am. Chem. Soc.* **2020**, *142*, 17167−17174.
(41) Cui, B.; Wang, H.; Ge, Q.; Zhu, X. Size-Dependent Strong Metal−Support Interactions of Rutile TiO_2-Supported Ni Catalysts for Hydrodeoxygenation of m-Cresol. *Catalysts* **2022**, *12*, 955.
(42) Zhang, Y.; Su, X.; Li, L.; Qi, H.; Yang, C.; Liu, W.; Pan, X.; Liu, X.; Yang, X.; Huang, Y.; Zhang, T. Ru/TiO_2 Catalysts with Size-Dependent Metal/Support Interaction for Tunable Reactivity in Fischer−Tropsch Synthesis. *ACS Catal.* **2020**, *10*, 12967−12975.
(43) Du, X.; Huang, Y.; Pan, X.; Han, B.; Su, Y.; Jiang, Q.; Li, M.; Tang, H.; Li, G.; Qiao, B. Size-dependent strong metal-support interaction in TiO_2 supported Au nanocatalysts. *Nat. Commun.* **2020**, *11*, No. 5811.
(44) Zhang, L.; Liu, X.; Wang, H.; Cao, L.; Huang, C.; Li, S.; Zhang, X.; Guan, Q.; Shao, X.; Lu, J. Size-dependent strong metal−support interaction in Pd/ZnO catalysts for hydrogenation of CO_2 to methanol. *Catal. Sci. Technol.* **2021**, *11*, 4398−4405.
(45) Liu, C.; Nauert, S. L.; Alsina, M. A.; Wang, D.; Grant, A.; He, K.; Weitz, E.; Nolan, M.; Gray, K. A.; Notestein, J. M. Role of surface reconstruction on Cu/TiO_2 nanotubes for CO_2 conversion. *Appl. Catal., B* **2019**, *255*, 117754.
(46) Du, W.; Zhang, Z.; Tang, Y.; Wang, Q.; Song, N.; Duan, X.; Zhou, X. Kinetic Insights into the Tandem and Simultaneous Mechanisms of Propylene Epoxidation by H_2 and O_2 on Au−Ti Catalysts. *ACS Catal.* **2023**, *13*, 2069−2085.
(47) Sinha, A. K.; Seelan, S.; Akita, T.; Tsubota, S.; Haruta, M. Vapor phase propylene epoxidation over Au/Ti-MCM-41 catalysts prepared by different Ti incorporation modes. *Appl. Catal., A* **2003**, *240*, 243−252.
(48) Yang, H.; Tang, D.; Lu, X.; Yuan, Y. Superior Performance of Gold Supported on Titanium-Containing Hexagonal Mesoporous Molecular Sieves for Gas-Phase Epoxidation of Propylene with Use of H_2 and O_2. *J. Phys. Chem. C* **2009**, *113*, 8186−8193.
(49) Sinha, A. K.; Seelan, S.; Tsubota, S.; Haruta, M. A Three-Dimensional Mesoporous Titanosilicate Support for Gold Nanoparticles: Vapor-Phase Epoxidation of Propene with High Conversion. *Angew. Chem.* **2004**, *116*, 1572−1574.
(50) Cumaranatunge, L.; Delgass, W. Enhancement of Au capture efficiency and activity of Au/TS-1 catalysts for propylene epoxidation. *J. Catal.* **2005**, *232*, 38−42.
(51) Li, W.; Chen, L.; Qiu, M.; Li, W.; Zhang, Y.; Zhu, Y.; Li, J.; Chen, X. Highly Efficient Epoxidation of Propylene with In Situ-Generated H_2O_2 over a Hierarchical TS-1 Zeolite-Supported Non-Noble Nickel Catalyst. *ACS Catal.* **2023**, *13*, 10487−10499.
(52) Wang, R.; Li, Y.; Shi, R.; Yang, M. Effect of metal−support interaction on the catalytic performance of Ni/Al_2O_3 for selective hydrogenation of isoprene. *J. Mol. Catal. A:Chem.* **2011**, *344*, 122−127.
(53) Lu, J.; Lei, Y.; Wan, G.; Mei, Z.; Yu, J.; Zhao, Y.; He, S.; Luo, Y. Weakening the metal-support strong interaction to enhance catalytic performances of alumina supported Ni-based catalysts for producing hydrogen. *Appl. Catal., B* **2020**, *263*, 118177.

https://doi.org/10.1021/acscatal.5c02681
ACS Catal. 2025, 15, 14741−14750

(54) Lu, R.; He, L.; Wang, Y.; Gao, X.-Q.; Li, W.-C. Promotion effects of nickel-doped Al_2O_3-nanosheet-supported Au catalysts for CO oxidation. *Chin. J. Catal.* **2020**, *41*, 350−356.
(55) Wu, Y.; Weckhuysen, B. M. Separation and Purification of Hydrocarbons with Porous Materials. *Angew. Chem., Int. Ed.* **2021**, *60*, 18930−18949.
(56) Bae, Y. S.; Lee, C. Y.; Kim, K. C.; Farha, O. K.; Nickias, P.; Hupp, J. T.; Nguyen, S. T.; Snurr, R. Q. High Propene/Propane Selectivity in Isostructural Metal−Organic Frameworks with High Densities of Open Metal Sites. *Angew. Chem., Int. Ed.* **2012**, *51*, 1857−1860.
(57) Vogt, C.; Monai, M.; Sterk, E. B.; Palle, J.; Melcherts, A. E. M.; Zijlstra, B.; Groeneveld, E.; Berben, P. H.; Boereboom, J. M.; Hensen, E. J. M.; Meirer, F.; Filot, I. A. W.; Weckhuysen, B. M. Understanding carbon dioxide activation and carbon−carbon coupling over nickel. *Nat. Commun.* **2019**, *10*, No. 5330.
(58) Vogt, C.; Groeneveld, E.; Kamsma, G.; Nachtegaal, M.; Lu, L.; Kiely, C. J.; Berben, P. H.; Meirer, F.; Weckhuysen, B. M. Unravelling structure sensitivity in CO_2 hydrogenation over nickel. *Nat. Catal.* **2018**, *1*, 127−134.
(59) Lin, D.; Lewis, R. J.; Feng, X.; Hutchings, G. J.Selective Oxidation by TS-1 coupled with in-situ Synthesised H_2O_2 *Fundam. Res.* 2024; Vol. *3* .

https://doi.org/10.1021/acscatal.5c02681
ACS Catal. 2025, 15, 14741−14750